Simulation of inverse Compton scattering and its implications on the scattered linewidth

N. Ranjan,[1] B. Terzić,[2,*] G. A. Krafft,[2,3] V. Petrillo,[4,5] I. Drebot,[4] and L. Serafini[4]

[1]*Princess Anne High School, Virginia Beach, Virginia 23462, USA*
[2]*Department of Physics, Center for Accelerator Science,*
Old Dominion University, Norfolk, Virginia 23529, USA
[3]*Thomas Jefferson National Accelerator Facility, Newport News, Virginia 23606, USA*
[4]*INFN-Milan, via Celoria 16, 20133 Milano, Italy*
[5]*Universita degli Studi di Milano, via Celoria 16, 20133 Milano, Italy*

Rising interest in inverse Compton sources has increased the need for efficient models that properly quantify the behavior of scattered radiation given a set of interaction parameters. The current state-of-the-art simulations rely on Monte Carlo–based methods, which, while properly expressing scattering behavior in high-probability regions of the produced spectra, may not correctly simulate such behavior in low-probability regions (e.g. tails of spectra). Moreover, sampling may take an inordinate amount of time for the desired accuracy to be achieved. In this paper, we present an analytic derivation of the expression describing the scattered radiation linewidth and propose a model to describe the effects of horizontal and vertical emittance on the properties of the scattered radiation. We also present an improved version of the code initially reported in Krafft *et al.* [Phys. Accel. Beams **19,** 121302 (2016)], that can perform the same simulations as those present in CAIN and give accurate results in low-probability regions by integrating over the emissions of the electrons. Finally, we use these codes to carry out simulations that closely verify the behavior predicted by the analytically derived scaling law.

I. INTRODUCTION

The increasing demand for efficient production of high-energy photons has resulted in interest in the construction of inverse Compton sources. In particular, the desire to create hard x rays from compact devices has propelled many groups worldwide to construct and improve such sources [1–10]. The primary attraction of these sources is that they are capable of yielding emissions with low bandwidths, which are desirable in various applications. It is thus necessary to study how certain interaction parameters of inverse Compton sources—the most important being the properties of the colliding electrons, the incident laser, and the aperture—affect the linewidth of scattered radiation. In the regime where electron recoil is negligible (Thomson regime), numerous studies provide analytical estimates of the dependence of the scattered linewidth (see [11–13], and references therein). In the same regime, an innovative scheme of laser chirping has been

devised to substantially decrease the linewidth of scattered radiation [14–17]. However, the regime where electron recoil is important (Compton regime) has not been scrutinized as closely, and, therefore, the effects of properties of the electron and photon beams on the scattering linewidth have so far remained largely unexplored [18]. In this paper, we analytically derive a scaling law for the linewidth of scattered radiation in the large electron recoil, low laser intensity (linear Compton) regime. We also present a numerical tool for the computation of scattered radiation spectra which is more accurate than the existing methods. These scaling results and the numerical tool may be instrumental when designing and optimizing Compton sources of many MeVs or GeVs, such as that described in Ref. [10].

Numerical simulations have been developed to study the performance of inverse Compton sources. The current standard used for such investigations is CAIN, a collection of codes used to model beam-to-beam interaction [19]. The main algorithm employed is MonteCarlo integration, for which rare events in nature will be as rare in the simulation. This means that the statistics in situations where low scattered photon counts are expected—for example, in the tails of the distribution or at very narrow apertures—will suffer from poor statistics. Our proposed code, the improved codes for Compton simulation (ICCS), will

---

overcome this problem by the nature of its formalism: The computed spectra of each individual electron-laser interaction will reflect the probabilities of photon scattering over the entire allowed range, providing statistics in the tails at the same level as in the peaks. ICCS can be used to simulate and verify the analytically derived radiation linewidth scaling laws, improving the estimates presented in Ref. [18].

The minimization of the bandwidth of scattered radiation is of key importance in all light sources. In Compton sources, it is necessary to consider the effects of all of the interaction parameters—the properties of the colliding electrons, the incident laser, and the aperture—on the bandwidth of scattered radiation in all regimes. By considering the behavior of the Compton formula (itself dependent on the electron recoil of the interaction, quantified by a unitless recoil factor X), we confirm analytically that the influence of the laser bandwidth and aperture is suppressed in regimes where electron recoil is substantial, as discussed in Ref. [18]. Therefore, it is only the properties of the electron beam that dominate the bandwidth of scattered radiation at high electron energies. An important consequence then arises, as first reported in Ref. [18]: When the electron recoil is substantial, the quality of the laser beam and the electron beam emittance is not as important as when the recoil can be neglected. However, electron beam energy spread remains important in all regimes of the recoil parameter.

The paper is organized as follows. In Sec. II, the scaling of scattered radiation bandwidth is discussed. The subsections describe, in order, mathematical derivations of a resultant scaling law, verification of the derived relation using numerical simulations of Gaussian laser beams when the electron recoil is negligible, moderate and substantial, and a discussion of applications, consequences, and limitations. In Sec. III, the computation of low-intensity Compton spectra using ICCS is outlined, and its intricacies are described in greater detail. In the subsections, we describe implementation improvements applied to the code and benchmark it against CAIN [19]. Finally, a discussion and summary of conclusions is provided in Sec. IV.

II. SCALING OF SCATTERED RADIATION LINEWIDTH

Understanding the scaling of scattered radiation bandwidth in Compton sources at high electron energies is a key goal of this investigation. In this section, we present a derivation of an analytic scaling law, test it against results from numerical simulations with ICCS, and consider its applicability and limitations. The key assumption is that the individual sources of linewidth are statistically independent, so the total spread of scattered energies can be expressed as a simple rms value.

A. Derivation of scaling law

The general Compton formula relating frequencies after scattering at some angle $0 \leq \theta \leq \theta_{\max}$ and energies of the incident electrons and photons, as given in Eq. (49) of Ref. [12], is

$$\omega'(\theta) = \frac{\omega(1 + \beta)}{1 - \beta\cos(\theta) + \{\hbar\omega/(\gamma m_e c^2)\}[1 + \cos(\theta)]}, \quad (1)$$

where ω is the incident laser frequency, $\omega'(\theta)$ is the scattered radiation frequency, c is the speed of light, β is the ratio of electron speed and the speed of light c: v_e/c, θ is the scattering angle, m_e is the rest mass of an electron, and $\gamma = E_e/(m_e c^2)$. At relativistic and ultra-relativistic energies (as is the case in Refs. [12,18]), $\beta \approx 1$.

It is also important to recall the definition of X, a representation of electron recoil in the collision [18]:

$$X = \frac{4E_e E_L}{(m_e c^2)^2}, \quad (2)$$

where E_e is the energy of the electron, E_L is the lab-frame energy of a counterpropagating photon, and $m_e c^2 \approx 511$ keV is the rest energy of an electron.

In order to obtain an expression in terms of X from Eq. (1), some algebraic manipulation is required using the identity $1/\gamma = \sqrt{1 - \beta^2}$, and

$$\omega'(\theta) = \frac{\omega(1 + \beta)^2 \gamma^2}{\gamma^2(1 - \beta\cos\theta)(1 + \beta) + \frac{X}{4}(1 + \cos\theta)(1 + \beta)}. \quad (3)$$

Using the first-order expansion $\cos(\theta) \approx 1 - \theta^2/2$, we obtain

$$\omega'(\theta) = \frac{\omega(1 + \beta)^2 \gamma^2}{1 + \frac{\beta(1+\beta)\gamma^2\theta^2}{2} + \frac{X(1+\beta)(2-\theta^2/2)}{4}}. \quad (4)$$

For $\beta \approx 1$, the expression reduces to

$$\omega'(\theta) \approx \frac{4\omega\gamma^2}{1 + X + \theta^2\gamma^2}, \quad (5)$$

since $\gamma^2 \gg X/4$. Expressing Eq. (5) in terms of energy rather than frequency yields

$$E'_{\text{ph}} = \frac{4E_L\gamma^2}{1 + X + \theta^2\gamma^2}, \quad (6)$$

where E'_{ph} is the scattered photon energy. We use this equation to derive the scattered energy spread from the aperture, electron beam energy spread, and photon energy

spread terms of the scaling law. The expression for the maximum scattered energy at the Compton edge can be obtained by setting $\theta = 0$:

$$E'_{ph,max} = \frac{4\gamma^2 E_L}{1 + X},\tag{7}$$

which is consistent with Eq. (7) presented in Ref. [18].

1. Dependence of linewidth on electron and photon beam bandwidth

The scattered energy spread generated by energy spreads in the electron beam and laser can be derived in a similar way. Taking the total derivative of Eq. (7) yields

$$dE'_{ph} = \frac{8\gamma E_L d\gamma}{1 + X} + \frac{4\gamma^2 dE_L}{1 + X} - \frac{4\gamma^2 E_L dX}{(1 + X)^2}.\tag{8}$$

Dividing by the result of Eq. (6) leads to

$$\frac{dE'_{ph}}{E'_{ph}} = \frac{2 + X}{1 + X}\frac{d\gamma}{\gamma} + \frac{1}{1 + X}\frac{dE_L}{E_L}.\tag{9}$$

This expression is valid only if γ and E_L are distributed as independent random variables, and for $\theta = 0$. A more general expression is obtained when taking the total derivative of Eq. (6) and evaluating the relative error:

$$\frac{dE'_{ph}}{E'_{ph}} = \frac{\sigma_\gamma}{E_\gamma} + \frac{\sigma_L}{E_L} - \frac{2(\gamma\theta)^2}{1 + X + (\gamma\theta)^2}\frac{d\theta}{\theta},\tag{10}$$

where

$$\frac{\sigma_\gamma}{E_\gamma} = \frac{2 + X}{1 + X + \psi^2}\frac{d\gamma}{\gamma},$$

$$\frac{\sigma_L}{E_L} = \frac{1 + \psi^2}{1 + X + \psi^2}\frac{dE_L}{E_L}.\tag{11}$$

These expressions introduce a modification to Eq. (9) on the order of $(\gamma\theta)^2$. While the modification may be negligible at small scattering angles, it becomes appreciable at larger angles. It should be cautioned that $d\theta/\theta$ is not the aperture term. This is because the dependence of the scattered linewidth on the aperture encompasses a wide range of scattering angles and is not dependent on the error of a single scattering event.

2. Dependence of linewidth on small apertures

To calculate the energy spread of the photons passing through an aperture, we must use the electron distribution function $dN/d\Omega(\theta)$ as a function of some scattering angle.

For small apertures, $\gamma\theta_{max} \ll 1$, the distribution can be approximated as uniform: $dN/d\Omega(0) \approx dN/d\Omega(\theta_{max})$
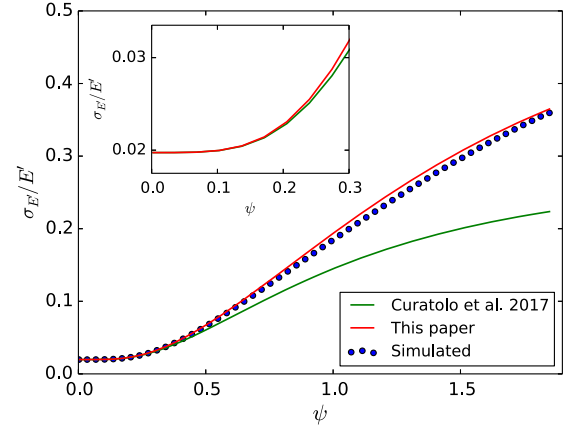

FIG. 1. The comparison between the scattering linewidth given by Eq. (14) of Ref. [18] (green line) and Eqs. (14) and (23) of this paper (red line), compared to the simulations with ICCS (blue dots). The simulation parameters are those given for case A_a in Sec. II B 3.

(see Fig. 2 in Ref. [12]). There is a one-to-one correspondence between scattering angle θ and scattered frequency ω, so the relative spread of one distribution is equivalent to the other. The variance $\sigma^2_{\theta_{max}}$ of a uniform distribution with bounds ω_{min} and ω_{max} is

$$\sigma^2_{\theta_{max}} = \frac{(\omega_{max} - \omega_{min})^2}{12}.\tag{12}$$

In order to calculate the relative spread, we must consider $\sigma^2_{\theta_{max}}$ and divide by a normalizing value $\omega_{mid} = (\omega_{max} + \omega_{min})/2$. This leads to Eq. (48) from [12]:

$$\frac{\sigma_{\theta_{max}}}{E_{\theta_{max}}} = \frac{\omega_{max} - \omega_{min}}{\sqrt{12}\omega_{mid}},\tag{13}$$

where $\sigma_{\theta_{max}}/E_{\theta_{max}}$ is the aperture relative energy spread [12]. Because $\omega_{max} = \omega'(0) = 4\omega\gamma^2/(1 + X)$ and $\omega_{min} = \omega'(\theta_{max}) = 4\omega\gamma^2/(1 + X + \psi^2)$, we can simplify the expression:

$$\frac{\sigma_{\theta_{max}}}{E_{\theta_{max}}} = \frac{1}{\sqrt{12}}\frac{\psi^2}{1 + X + \psi^2/2},\tag{14}$$

where $\psi = \gamma\theta_{max}$. This expression is different (there is a factor of $1/2$ attached to ψ^2 in the denominator) from the analogous term reported in Ref. [18]. At small apertures ($\psi^2 \ll X$), the difference is negligible, as can be seen in Fig. 1. However, as the aperture grows, the scaling law reported in Ref. [18] becomes increasingly inaccurate. The agreement between our new analytical scaling law and the numerical simulations is excellent at all apertures.

A second-order correction to the aperture linewidth in Eq. (14) is given in the Appendix.

3. Dependence of linewidth on emittance at small apertures

Consider the generalized Compton formula in Eq. (6) in a backscattering arrangement for an electron that is not aligned with the observation angle of the beam. (The z axis in this case is the direction of the average beam velocity, so the mean nonaligned momentum should remain zero.) Consider some $\theta_r = \sqrt{\theta_x^2 + \theta_y^2}$ by which an electron is misaligned. Then Eq. (6) becomes

$$E'_{\rm ph}(\theta_x, \theta_y) = \frac{4E_L\gamma^2}{1 + X + \gamma^2(\theta_x^2 + \theta_y^2)} \quad (15)$$

for the energy of the photon radiated to the center of the aperture. It is also reasonable to assume that the distribution ρ of horizontal and vertical angles follows a bivariate normal distribution with no cross-correlation:

$$\rho(\theta_x, \theta_y) = \frac{1}{2\pi\sigma_{\theta_x}\sigma_{\theta_y}} \exp\left(-\frac{\theta_x^2}{2\sigma_{\theta_x}^2} - \frac{\theta_y^2}{2\sigma_{\theta_y}^2}\right). \quad (16)$$

So, in addition to the electron beam energy spread σ_E/E_e, the linewidth is impacted by some $\sigma_\epsilon/E_\epsilon$ that is obtained by solving for the second moment of the emittance angle-dependent function, given in Eq. (15), and collecting the terms up to the fourth order. Recalling that the fourth moment of a standard normal distribution is $3\sigma^4$, we obtain

$$\langle E'_{\rm ph}\rangle = \iint_{-\infty}^{\infty} E'_{\rm ph}(\theta_x, \theta_y)\rho(\theta_x, \theta_y)d\theta_x d\theta_y$$

$$\approx E'_{\rm ph,max}\left(1 - \frac{\gamma^2(\sigma_{\theta_x}^2 + \sigma_{\theta_y}^2)}{1 + X}\right. $$

$$\left. + \frac{\gamma^4(3\sigma_{\theta_x}^4 + 2\sigma_{\theta_x}^2\sigma_{\theta_y}^2 + 3\sigma_{\theta_y}^4)^2}{(1 + X)^2}\right), \quad (17)$$

$$\langle E'^2_{\rm ph}\rangle = \iint_{-\infty}^{\infty} E'^2_{\rm ph}(\theta_x, \theta_y)\rho(\theta_x, \theta_y)d\theta_x d\theta_y$$

$$\approx E'^2_{\rm ph,max}\left(1 - \frac{2\gamma^2(\sigma_{\theta_x}^2 + \sigma_{\theta_y}^2)}{1 + X}\right.$$

$$\left. + \frac{3\gamma^4(3\sigma_{\theta_x}^4 + 2\sigma_{\theta_x}^2\sigma_{\theta_y}^2 + 3\sigma_{\theta_y}^4)}{(1 + X)^2}\right). \quad (18)$$

Using the results of Eqs. (17) and (18) in the definition of variance yields

$$\frac{\sigma_\epsilon^2}{E_\epsilon^2} = \frac{\langle E'^2_{\rm ph}\rangle - \langle E'_{\rm ph}\rangle^2}{\langle E'_{\rm ph}\rangle} = \frac{2\gamma^4(\sigma_{\theta_x}^4 + \sigma_{\theta_y}^4)}{(1 + X)^2}. \quad (19)$$

Noting $\sigma_{\theta_x} = \sqrt{\epsilon_x/\beta_x^*}$ and $\sigma_{\theta_y} = \sqrt{\epsilon_y/\beta_y^*}$, we obtain

$$\frac{\sigma_\epsilon}{E_\epsilon} = \sqrt{\left(\frac{\sigma_{\epsilon_x}}{E_{\epsilon_x}}\right)^2 + \left(\frac{\sigma_{\epsilon_y}}{E_{\epsilon_y}}\right)^2}$$

$$= \frac{\sqrt{2}\gamma^2}{1 + X}\sqrt{\frac{\epsilon_x^2}{\beta_x^{*2}} + \frac{\epsilon_y^2}{\beta_y^{*2}}}. \quad (20)$$

Therefore, for small apertures, the bandwidth due to emittance becomes increasingly negligible as electron recoil becomes more important. However, in regimes where the recoil is negligible ($X \approx 0$), the bandwidth of scattered radiation could very well be dominated by emittances. This expression is a generalization of the expressions given in Refs. [1,12,18]. For symmetric distributions, $\epsilon_x = \epsilon_y \equiv \epsilon$ and $\beta_x^* = \beta_y^* \equiv \beta^*$, and for the negligible values of the recoil parameter X, the above equation reduces to the unnumbered equation in Ref. [1], Eq. (50) in Ref. [12], and Eq. (13) in Ref. [18]:

$$\frac{\sigma_\epsilon}{E_\epsilon} = \frac{2\gamma^2\epsilon}{\beta^*}. \quad (21)$$

4. Revised scaling law

As the terms for electron energy spread, photon energy spread, and aperture energy spread are independent, a simple rms value can be used to calculate the relative bandwidth of radiation [12,18]. The final expression is given by

$$\frac{\sigma_{E'_{\rm ph}}}{E'_{\rm ph}} = \sqrt{\left(\frac{\sigma_{\theta_{\rm max}}}{E_{\theta_{\rm max}}}\right)^2 + \left(\frac{\sigma_\gamma}{E_\gamma}\right)^2 + \left(\frac{\sigma_L}{E_L}\right)^2 + \left(\frac{\sigma_\epsilon}{E_\epsilon}\right)^2}, \quad (22)$$

where the individual terms are given in Eqs. (14), (11), and (20). The scaling law in Ref. [18] also features two additional terms—one that measures the beam quality and the other the ponderomotive broadening in the photon field. Those two terms are beyond the scope of this paper. In the limit $\psi \ll 1$, the electron and photon beam terms are in agreement with the more general Eq. (14) of Ref. [18], which is valid for all ψ. However, a modification to the aperture term (an added factor of $1/2$ in the denominator) is required to accurately model the energy spread in regimes at larger apertures. Finally, a term containing the emittance models the change in the energy spread for Gaussian spectra.

For non-Gaussian spectra skewed by emittance effects, it has been suggested that covariance between the aperture and emittance must be accounted for. Equation (14) of Ref. [18] suggests that instead the emittance and aperture are combined before squaring:

$$\frac{\sigma_{E'_{\rm ph}}}{E'_{\rm ph}} = \sqrt{\left(\frac{\sigma_{\theta_{\rm max}}}{E_{\theta_{\rm max}}} + \frac{\sigma_\epsilon}{E_\epsilon}\right)^2 + \left(\frac{\sigma_L}{E_L}\right)^2 + \left(\frac{\sigma_\gamma}{E_\gamma}\right)^2}. \quad (23)$$

An intuitive reason for doing so can be arrived at when considering the misaligned electrons that are accelerated through the aperture. If the emittances become too large, the small aperture in these simulations can result in radiated energy possessing different scattering angles (and thus energies) that skew the spectrum. In this way, there is demonstrated a dependence between the aperture and emittances as the probabilistic frequency of certain energies is greatly reduced. The few photons emitted with those corresponding energies make the characteristic tail observed. This reasoning also demonstrates why spectra of scattered radiation are always skewed toward smaller energies, since any deviation in the direction of the mean electron energy will result in a lower scattered frequency. For lower emittances, however, there is a smaller likelihood for the aperture to change the behavior of the incident electron, which makes them nearly independent. The numerical verification of the covariance in the scaling law is reported in Sec. II B 4.

B. Computational validation of the scaling law

To verify the accuracy of the derived terms, Eq. (23) was compared to the calculated bandwidth from a spectrum produced using the ICCS code described in detail in Sec. III. The energies of cases D, E, and F of Ref. [18] (shown in Table I) are used in the simulations, only with differing interaction parameters. They are distinguished with appropriate subscripts for photon beam bandwidth, electron beam bandwidth, aperture, and emittance (given in Tables II–VI). Additional cases with either very small or very large X were used to highlight the modification to the scaling law made in Sec. II. Both Eqs. (22) and (23) were considered in the context of emittances.

1. Dependence of linewidth on photon beam bandwidth

Cases D, E, and F from Ref. [18] were directly used to verify the scaling of Eq. (23) and here are referred to as

TABLE I. Electron energies, laser beam wavelengths, and the resulting recoil parameters for cases D, E, and F from Ref. [18].

Case	E_e [GeV]	λ [nm]	X
D	7	10^3	0.133
E	7	10	13.3
F	7	0.1	1330

TABLE II. Parameters used to verify the scaling of photon energy, separated by case.

Case	E_e [GeV]	λ [nm]	X	$\frac{\sigma_\gamma}{E_\gamma}$	$\theta_{\max}$
D_{la}	7	10^3	0.133	0	5×10^{-6}
E_{la}	7	10	13.3	0	1.33×10^{-5}
F_{la}	7	0.1	1330	0	2.67×10^{-5}

TABLE III. Parameters used to verify the scaling of electron energy, separated by case.

Case	E_e [GeV]	λ [nm]	X	$\frac{\sigma_L}{E_L}$	$\theta_{\max}$
D_{el}	7	10^3	0.133	2×10^{-4}	5×10^{-6}
E_{el}	7	10	13.3	2×10^{-4}	1.33×10^{-5}
F_{el}	7	0.1	1330	2×10^{-4}	2.67×10^{-5}

TABLE IV. Parameters used to verify the scaling of the aperture, separated by case.

Case	E_e [GeV]	λ [nm]	X	$\frac{\sigma_\gamma}{E_\gamma}$	$\frac{\sigma_L}{E_L}$
A_a	7	10^4	0.0133	0	2×10^{-2}
D_a	7	10^3	0.133	0	2×10^{-2}
E_a	7	10	13.3	0	2×10^{-2}
F_a	7	0.1	1330	0	2×10^{-2}

TABLE V. Parameters used to verify the scaling of the emittance, separated by case.

Case	E_e [GeV]	λ [nm]	X	$\frac{\sigma_L}{E_L}$	$\frac{\sigma_\gamma}{E_\gamma}$	$\theta_{\max}$
$D_{em,1}$	7	10^3	0.133	2.25×10^{-3}	0	8.33×10^{-7}
$D_{em,2}$	7	10^3	0.133	2.25×10^{-3}	0.002	8.33×10^{-7}
$E_{em,1}$	7	10	13.3	2.25×10^{-3}	0	1.33×10^{-6}
$E_{em,2}$	7	10	13.3	2.25×10^{-3}	0.0002	1.33×10^{-6}

TABLE VI. Parameters used to verify the scaling of the emittance for non-Gaussian spectra for large apertures, separated by case. Emittances in these cases are larger than those in Table IV and thus skew the spectrum so that asymmetry is clearly observable.

Case	E_e [GeV]	λ [nm]	X	$\frac{\sigma_L}{E_L}$	$\frac{\sigma_\gamma}{E_\gamma}$	$\theta_{\max}$
$D_{em,3}$	7	10^3	0.133	2.25×10^{-3}	0	10^{-5}
$D_{em,4}$	7	10^3	0.133	2.25×10^{-3}	0	10^{-6}

cases D_{la}, E_{la}, and F_{la}, respectively, and shown in Table II. The energy spread of the incident radiation diminishes and is eventually removed at large electron recoil regimes [since the prefactor $1/(1 + X) \to 0$ as X becomes large].

In other publications, energy spread may have been given by the width of the laser. It has been shown [12] that in a Gaussian model, for some width σ, the relative energy spread of the laser pulse is

$$\frac{\sigma_L}{E_L} = \frac{1}{2\sqrt{2\pi}\sigma}. \tag{24}$$

Other parameters were chosen so that they would have as small an effect on the scattered radiation bandwidth as possible. This included the assumption of perfect accuracy in the electron beam (which itself included the assumption of zero emittances in any direction).

Figure 2 shows an excellent agreement in the scaling law between the analytical expression given in Eq. (23) and the simulations using the code outlined in Sec. III.

2. Dependence of linewidth on electron beam bandwidth

Cases D, E, and F from Ref. [18] were directly used to verify the scaling of Eq. (23) and here are referred to as cases D_{el}, E_{el}, and F_{el}, respectively, and shown in Table III. The electron beam spread will always be a non-negligible factor in determining the scattered radiation bandwidth, although its impact is lessened by a factor of 2 in large electron recoil regimes [because $(2 + X)/(1 + X) \to 1$ for large X].

The photon beam bandwidth and the aperture were set to minimal values so that electron beam effects could be highlighted. Emittances in all directions were also set to zero—though these two factors are independent. Excellent agreement in the scaling law between the analytical expression given in Eq. (23) and the simulations using the code outlined in Sec. III is shown in Fig. 3.

3. Dependence of linewidth on aperture

A case where the recoil is negligible ($X = 0.013\,28$)—referred to here as case A—is used to demonstrate more pronounced deviations as $\gamma\theta$ approaches 1, in addition to cases D, E, and F from Ref. [18]. They are shown in Table IV. As the electron recoil becomes large, the overall effect of the aperture on the scattered linewidth is essentially removed as the term $\psi^2/(1 + X)$ approaches zero.

Figure 4 shows excellent agreement in the scaling law between the analytical expression given in Eq. (23) and the simulations using the ICCS code outlined in Sec. III. As large electron recoil regimes are approached, the dependence of the scattered radiation linewidth on the aperture becomes more suppressed as X dominates. Unlike the scaling of the photon energy spread, electron beam energy spread, and emittance, the relationship is quadratic rather than linear. When the electron recoil is taken into account, the aperture must be increased to observe the resultant spectra.

4. Dependence of linewidth on emittance at small apertures

Cases D and E from Ref. [18] were used to consider the scaling of the emittance against the scattered radiation bandwidth and are given in Table V. Two cases for each energy were then considered: one with zero mean incident electron beam energy spread and one with nonzero mean energy spread. In extremely large recoil regimes, the
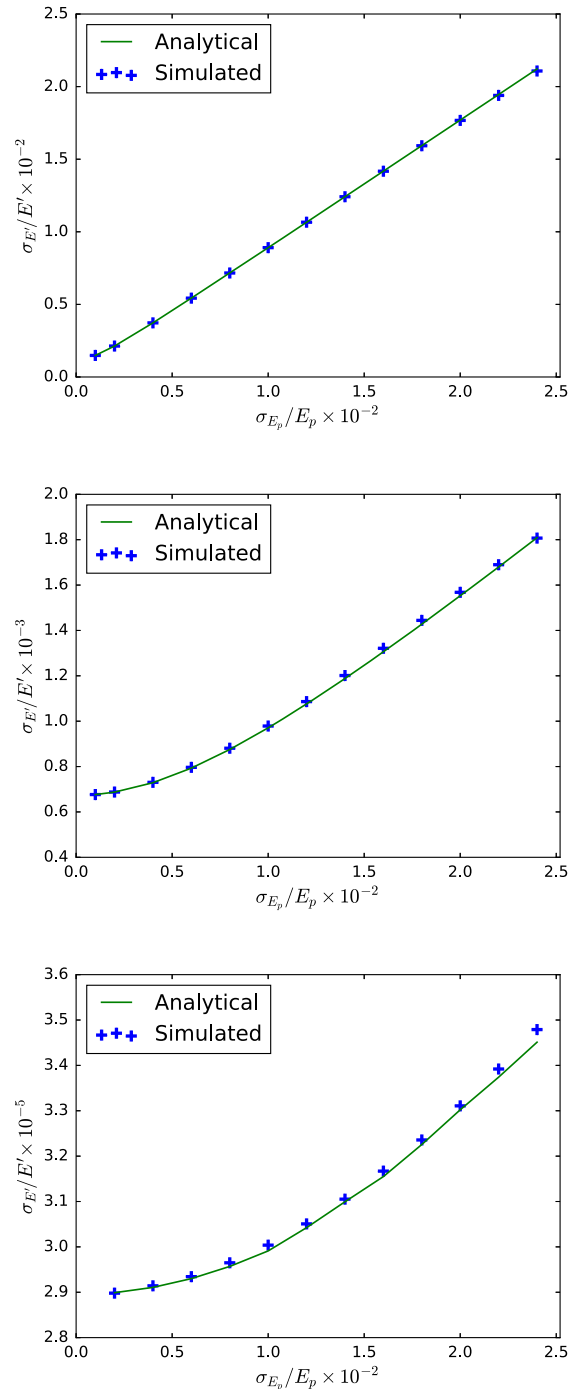

FIG. 2.   Relationship between the energy spread of photon beam σ_L/E_L and the resulting linewidth of scattered radiation. Electron beam energy spread is held constant at $\sigma_\gamma/E_\gamma = 0$ and emittance at $\epsilon_{x,y} = 0$. Panels represent cases D_{la}–F_{la}, given in Table II, from top to bottom. Results given in Eq. (23) are labeled "analytical." Numerical simulations carried out with ICCS are labeled "simulated." Panels are not on the same scale.

emittance will approach zero as the increasing of γ is surpassed by the increase in X. However, emittances chosen for Fig. 5 do not approach this regime, as it would require the frequencies to approach the Compton
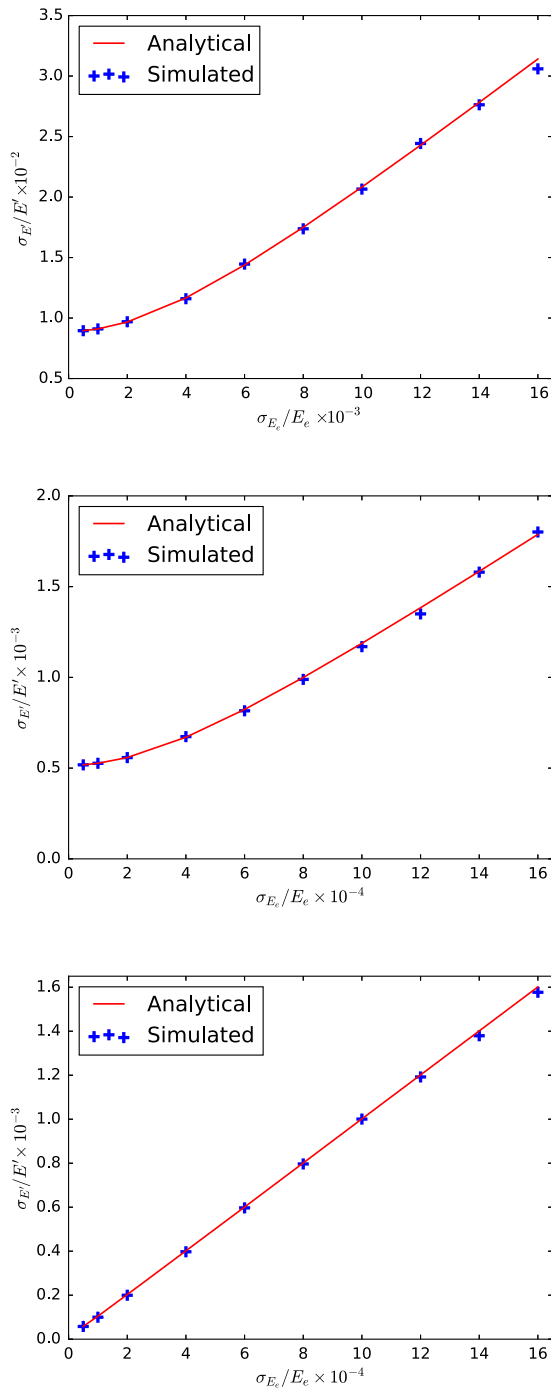
FIG. 3. Relationship between the energy spread of electron beam σ_γ/E_γ and the resulting linewidth of scattered radiation. Photon beam energy spread is held constant at $\sigma_L/E_L = 2 \times 10^{-4}$ and emittance at $\epsilon_{x,y} = 0$. Panels correspond to cases D_{el}–F_{el}, given in Table III, from top to bottom. The impact of electron beam spread is nearly halved in large electron recoil regimes. Values were chosen so that electron beam bandwidth dominated the linewidth of scattered radiation. Results given in Eq. (23) are labeled analytical. Numerical simulations carried out with ICCS are labeled simulated. Panels are not on the same scale.

frequency, which is in the γ-ray range for electrons [20]. Emittances were selected so that the spectra of scattered radiation were produced at small apertures, since the scaling deviates by greater amounts as the spectra become skewed half-Gaussian functions [11,12] and there is an increasing dependence between the emittance and aperture. Figure 5 shows excellent agreement in the scaling law between the analytical expression given in Eq. (23) and the simulations using the codes outlined in Sec. III.

Numerical simulations were carried out only with horizontal emittances ϵ_x, but for vertical emittances ϵ_y results were found to be very similar. The combination of both horizontal and vertical emittances could also be accounted for, as the emittance scaling factor is dependent on total emittance rather than emittances in any direction. It can be observed that the emittances do not scale as accurately as the other factors. This is because the model of emittance depends on a random variation in electron momenta and that larger skews in the distribution cause the bandwidth to be larger than predicted due to the increasing covariance between the aperture and emittance.

5. Dependence of linewidth on the covariance between aperture and emittance

Figure 6 shows the scaling law given in Eq. (23), which features a covariance between the aperture and emittance—first introduced in Eq. (14) of Ref. [18]—is a more accurate model for the rms spread of skewed spectra.

It appears that all four cases—modification of the photon energy spread, electron energy spread, aperture, and emittances—agree quite well in all energy regimes with the scaling law described in Eq. (22) in the case of Gaussian spectra, while they agree fairly well with Eq. (23) in the case of skewed spectra. An important consequence arises due to the presence of recoil factor X: The aperture and laser precision need not be too great.

III. COMPUTATION OF LOW-INTENSITY COMPTON SPECTRA

The current, state-of-the-art codes for the computation of low-intensity Compton spectra is CAIN, described as a "stand alone, Monte Carlo code for interaction involving high-energy electrons, photons, and positrons" [19]. It is able to compute high-energy interactions that involve Coulomb fields, luminosity between beams, synchrotron radiation, polarizations, and nonlinear effects of field strength [19]. Using the appropriate Lorentz transforms, simulations of random events over many trials can model the behavior of scattered radiation.

In this section, we report on the improved version of the code initially reported in Ref. [12], which we now call ICCS, and benchmark it against CAIN.
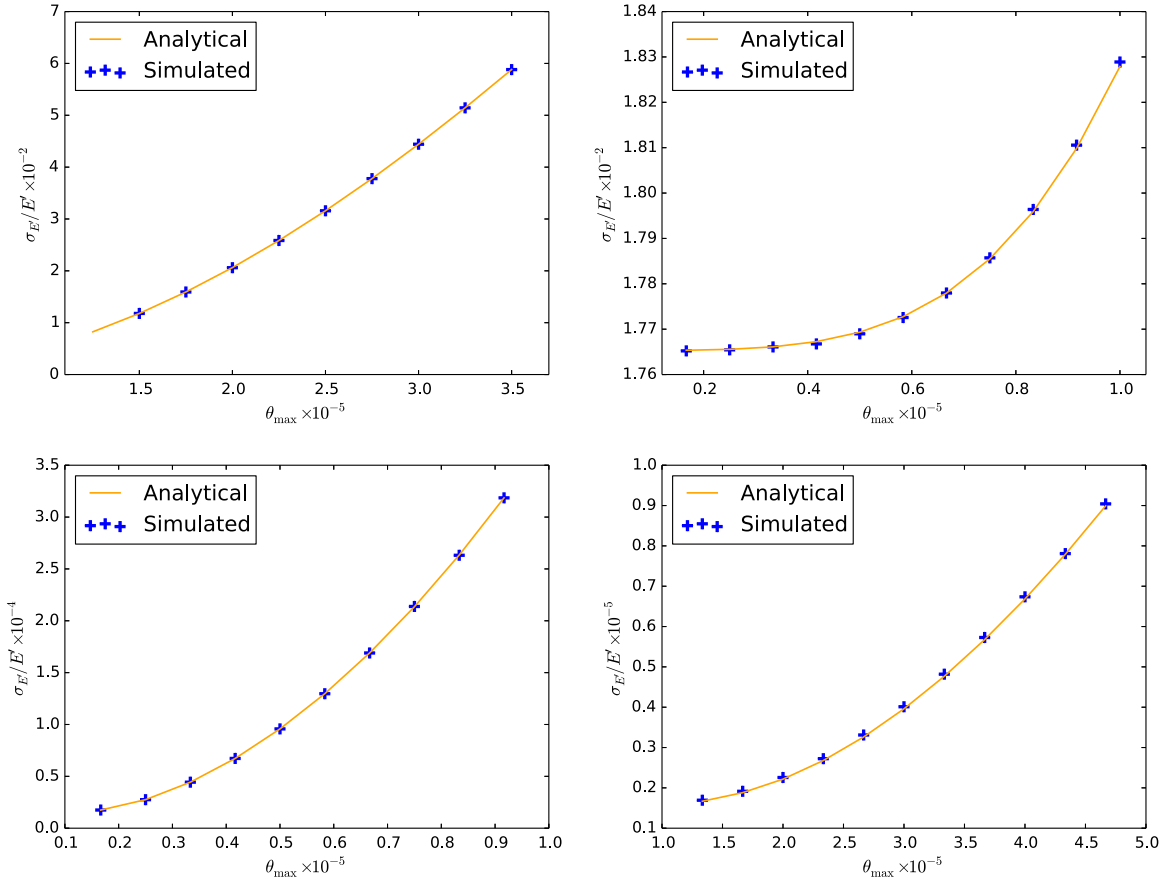
FIG. 4.   Relationship between the aperture and resulting linewidth of scattered radiation. The electron beam energy spread is held constant at $\sigma_\gamma/E_\gamma = 0$ and emittance at $\epsilon_{x,y} = 0$, photon beam at $\sigma_L/E_L = 2 \times 10^{-2}$. Parameters for all cases are reported in Table IV. Results given in Eq. (23) are labeled analytical. Numerical simulations carried out with ICCS are labeled simulated. Panels are not on the same scale. Top row (left to right): Cases A_a and D_a. Bottom row: Cases E_a and F_a.

A. ICCS: Improved code for Compton simulation

An earlier version of our code was described in detail in Ref. [12]. The code models the effects of the electromagnetic field through the normalized vector potential and uses it as an input to the simulations. The finite pulse effects possible in a real laser pulse are described properly within a plane-wave approximation. The width and energy of the laser are also given as input. To describe the properties of the incident electrons, the program receives the relative spread in energy σ_E/E_e, horizontal and vertical emittances ϵ_x and ϵ_y, and the value of the electron β_x and β_y functions evaluated at the interaction points (denoted by β_x^* and β_y^*). Finally, the range and location of sampling can be altered to consider various sections of the generated spectra. The algorithm implemented by our code overcomes a serious problem posed when using Monte Carlo integration: As the rarity of low-probability scatterings is reflected exactly in the code, results may suffer from poor statistics. Any electron distribution can be input and easily integrated according to Eq. (33) of Ref. [12]:

$$\frac{dU_1}{d\omega'} = \frac{\epsilon_0 c}{2\pi} \int_0^{2\pi} d\phi \int_{\cos\theta_{\max}}^1 |\tilde{E}[\omega(\omega')]|^2 \frac{d\sigma}{d\Omega} \left[\frac{\omega'}{\omega}\frac{d\omega}{d\omega'}\right] d(\cos\theta),$$

$$(25)$$

where $dU_1/d\omega'$ represents the differential scattered spectrum value, ϕ represents the solid scattering angle, and $\tilde{E}[\omega(\omega')]$ represents the time transform of the electron field. After summing over many particles ($N_p > 2000$), an extremely precise spectral distribution is given.

1. Improvement in electron distribution sampling

In the initial version of the code, distributions of electrons—horizontal, vertical, and longitudinal momenta p_x, p_y, and p_z, respectively—are generated as normally distributed in transverse (horizontal p_x and vertical p_y) and total momenta (p). In this approach, we specify as input (i) the horizontal and vertical emittances ϵ_x and ϵ_y, which determine the transverse momenta, and (ii) the magnitude
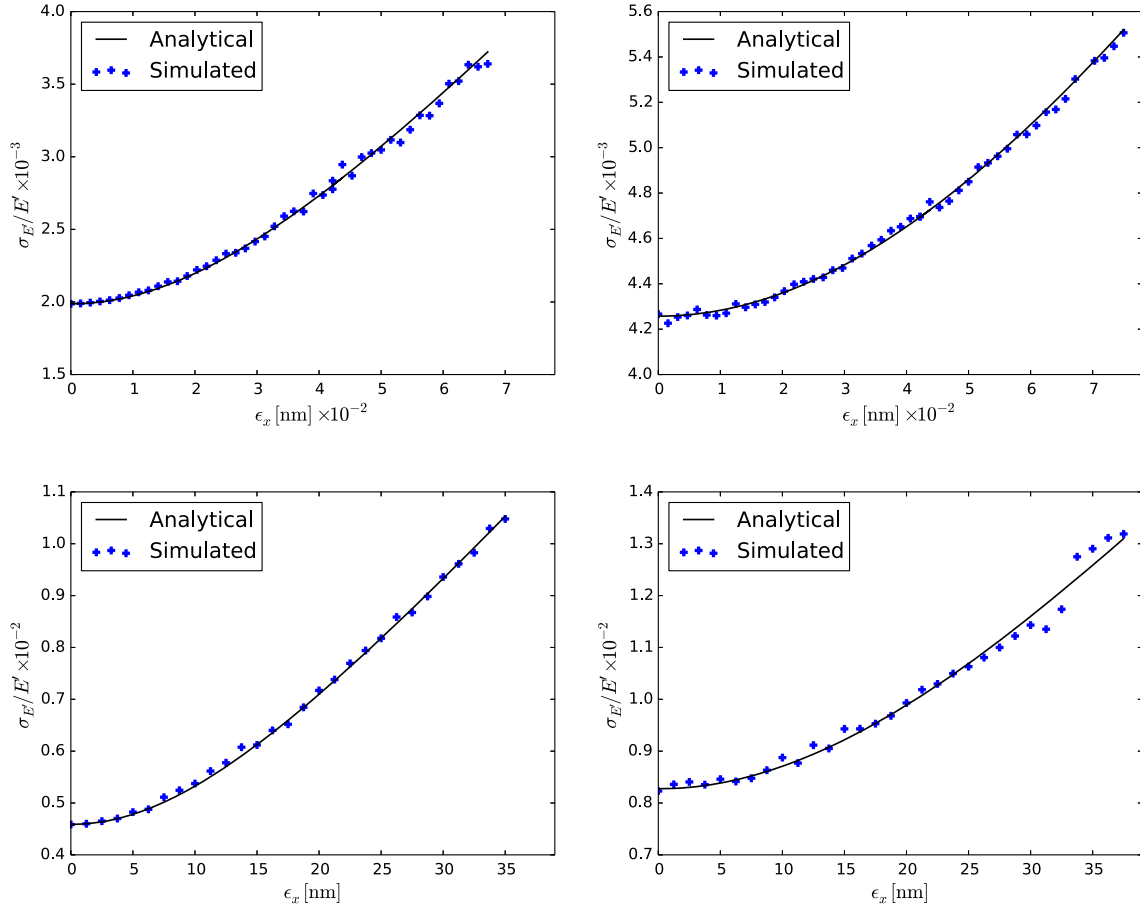
FIG. 5.   Relationship between the horizontal emittance of the electron beam ϵ_x and the resulting linewidth of scattered radiation. Parameters for all cases are reported in Table V. Analytical results given in Eq. (23) are labeled analytical. Numerical simulations carried out with ICCS are labeled simulated. Panels are not on the same scale. Top row (left to right): Cases $D_{em,1}$ and $D_{em,2}$. Bottom row: Cases $E_{em,1}$ and $E_{em,2}$.

of the total momentum $p = \sqrt{p_x^2 + p_y^2 + p_z^2}$ and the associated standard deviation σ_p, which is used to obtain the longitudinal momentum distribution:

$$p_x = N\left(0, \frac{\epsilon_x}{\beta_x^*}\right),$$

$$p_y = N\left(0, \frac{\epsilon_y}{\beta_y^*}\right),$$

$$p_z = \sqrt{[N(0, \sigma_p^2) + p]^2 - p_x^2 - p_y^2}.$$

$N(0, \sigma^2)$ represents a normal random variable with mean 0 and variance σ^2. The energy of individual electrons is found from the relativistic energy-momentum relation

$$E = \sqrt{p^2 c^2 + m_e^2 c^4} \qquad (26)$$

and then averaged to obtain the mean energy of the electron distribution E_0. The relative energy spread σ_E/E can then be computed either directly or from the relation

$$\sigma_p = \frac{1}{c}\sqrt{\left[E_0\left(1 + \frac{\sigma_E}{E}\right)\right]^2 - m^2 c^4} - p. \qquad (27)$$

Equation (27) is obtained from a first degree approximation to the σ_p given σ_E and using the relativistic energy-momentum relationship. This method is advantageous, as it allows for the user to dictate the relative energy spread of the electron beam—as is usually the case in a laboratory setting. Unfortunately, the assumptions made in the derivation of Eq. (27) may mean that runs at high emittances can deviate from theoretical predictions.

To combat this issue, ICCS uses another approach in which distributions of electrons are generated as normally distributed in horizontal, vertical, and longitudinal momenta—p_x, p_y, and p_z, respectively. In this approach, we specify as input (i) the horizontal and vertical emittances ϵ_x and ϵ_y, which determine the respective transverse momenta, and (ii) the magnitude of the longitudinal momentum p_z and the associated standard deviation σ_{p_z}, which is used to obtain the longitudinal momentum distribution:
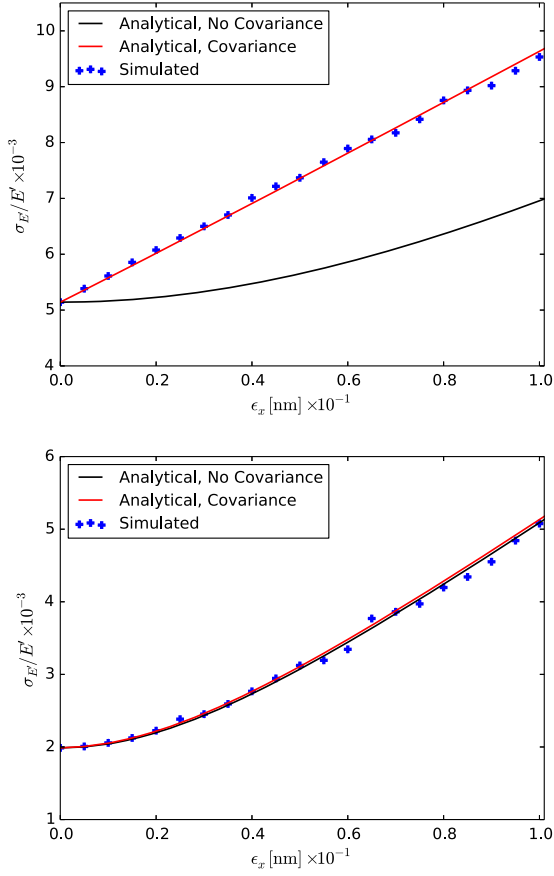
FIG. 6. Relationship between the emittance and resulting linewidth of scattered radiation. Top: Case $D_{\text{em},3}$. Bottom: Case $D_{\text{em},4}$. Including covariance, given in Eq. (23) and labeled analytical, covariance, does predict better in the regime of asymmetrical spectra than the case without covariance, given in Eq. (22), and labeled analytical, no covariance. Apertures were increased greatly to make the covariance more pronounced (top panel). For small apertures (bottom panel), the curve with covariance rises less sharply and closely follows the curve without covariance. Parameters for all cases are reported in Table VI.

$$p_x = N\left(0, \frac{\epsilon_x}{\beta_x^*}\right),$$

$$p_y = N\left(0, \frac{\epsilon_y}{\beta_y^*}\right),$$

$$p_z = N(p_z, \sigma_{p_z}).$$

As in the first approach, the energy of individual electrons is found from the relativistic energy-momentum relation given in Eq. (26) and then averaged to obtain the mean energy of the electron distribution E_γ. Then the relative energy spread σ_γ/E_γ can be computed either directly or from the relation in Eq. (27). In this way, the energy of the simulation can still be indirectly controlled. The obvious drawback of this approach is that the emittances and energy spread of the electron beam cannot both be directly controlled.

Another feature of the code is its ability to read in an arbitrary electron beam distribution as an input to the simulation. This is of particular importance when a specific electron beam distribution is given—for example, from a start-to-end simulation of inverse Compton sources [12].

The resulting spectra are subject to the central limit theorem (with the exception of high emittances that skew the distribution), and, therefore, high-precision simulations can be performed even with a relatively small number of particles. One can use the rough rule of thumb that accuracies of computed spectra vary inversely with the square root of the number of particles. Thus, for instance, only 400 particles would be needed for an average error of 5% in computed values [12].

2. Improvement in efficiency and implementation

The original version of the code, described in Ref. [12], was originally written in the PYTHON programming language [21]. PYTHON provides users with an easy and straightforward means of formula-to-code conversion. Unfortunately, the ease associated with its use translates to significantly increased run times due to the dynamically typed objects and convenient yet scattered memory allocation system [22]. To alleviate this issue, two tasks were undertaken. First, the program was parallelized using PYTHON's multiprocessing library to as many cores as the host computer could provide. Second, the CYTHON programming extension was used to provide the capabilities of the C language while retaining the advantages provided by PYTHON. The new version of the code (compared to the original PYTHON version) is anywhere from 8 to 30 times faster. Integration is still done with SCIPY's quad pack [23,24]. Unfortunately, this integrator may prove not to be optimal in cases where extremely precise integration is needed—it subsequently goes through many iterations to guarantee accuracy and slows the program down. Efforts for the new qag integrator with such capabilities are underway [12,24]. The ICCS code consists of a driver (through which all necessary parameters are input) and a CYTHON class that stores all the computation-intensive routines.

B. Comparison of ICCS and CAIN

We compared the results of the two codes—our new code ICCS and CAIN. Case D from Ref. [18], shown in Table VII, was used for a comparison. ICCS was executed at three different resolutions in terms of particles simulating

TABLE VII. Case D from Ref. [18] used as the standard to compare the two codes.

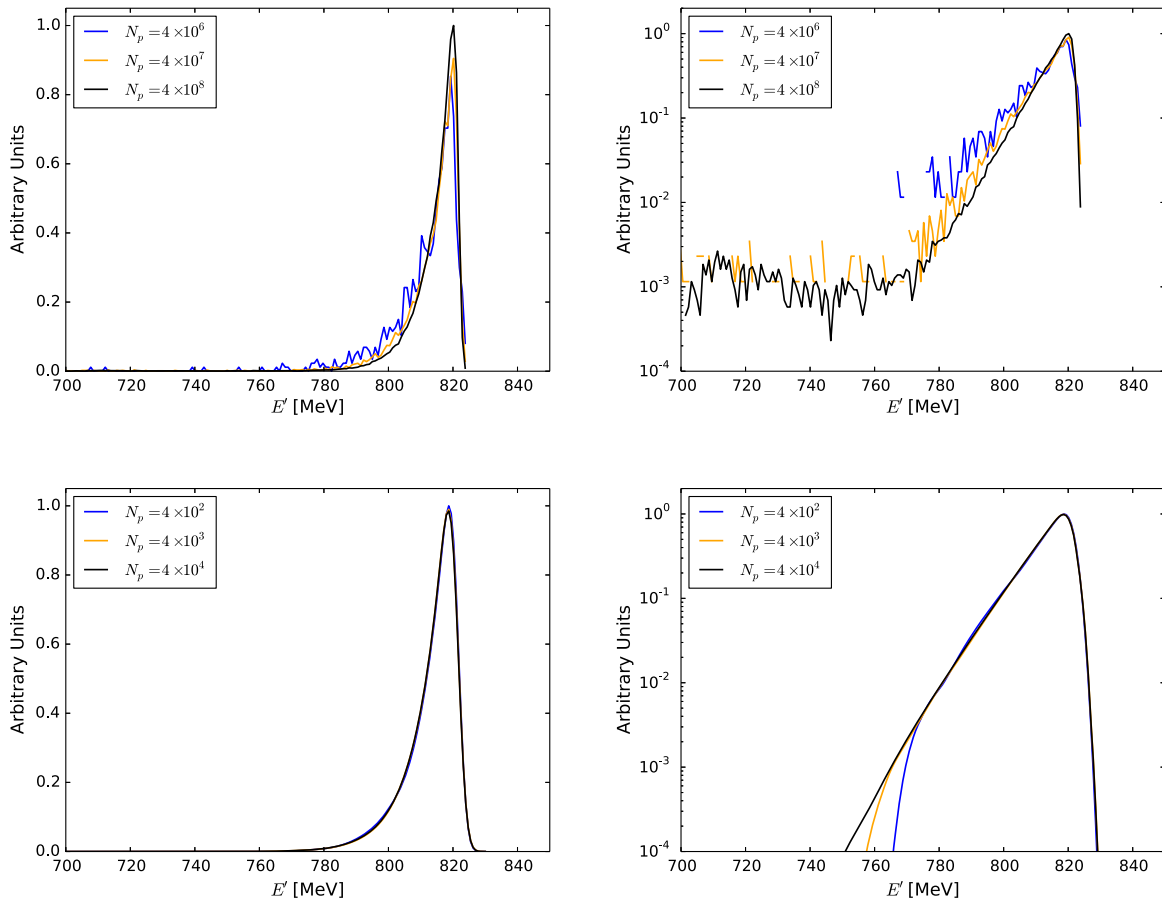| E_e [GeV]	λ [nm]	X	σ	$\epsilon_{\text{n},x} = \epsilon_{\text{n},y}$ [m]	$\frac{\sigma_\gamma}{E_\gamma}$	$\theta_{\max}$
7	10^3	0.133	50	4×10^{-7}	0.0008	5×10^{-6}

FIG. 7. The numerically simulated spectrum for increasing resolutions for CAIN [19] and ICCS for the case given in Table VII. The number of macroparticles N_p samples the electron beam distribution. Top row: CAIN simulations on the linear (left) and log scale (right). Bottom row: ICCS simulations on the linear (left) and log scale (right).

electrons: 400, 4000, and 40 000. CAIN was also executed at three different resolutions in terms of particles simulating electrons. At the end, the scaling estimates were compared.

Figure 7 shows the results produced by the two codes. It can be observed that the simulations with ICCS, compared to those carried out with CAIN, are superior in two main ways: (i) Continuous spectra are produced with accurate probabilities; and (ii) low-probability regions (tails) are modeled with a much higher accuracy, as can be seen by comparing the top and bottom right panels in Fig. 7.

IV. SUMMARY AND DISCUSSION

This paper addresses two key issues: (i) the scaling of the scattered radiation linewidth and (ii) the efficient and accurate simulation of inverse Compton scattering spectra in the low-intensity regime.

We have presented derivations of the terms of the scaling law reported in Eq. (14) of Ref. [18]. These terms are accurate approximations of a complete scaling law as given in Eq. (23) for the linear-field (low laser intensity) regime. We report a small correction to the aperture term which

becomes important at large apertures. We have also proposed a model for low-to-moderate emittance levels and have demonstrated computationally that there is a dependence between apertures and emittances (at high values). Finally, numerical simulations carried out with many particles verify the greater degree of accuracy of the altered scaling law.

We have also presented verification of certain aspects of the scaling law, which was first derived in Ref. [18] using simulations with a Monte Carlo code CAIN. While the evaluations in the high-probability portions of the spectrum of scattered radiation are generally accurate, those algorithms suffer from poor statistics in low-probability regions like the tails of the spectrum. The calculation of spectra with CAIN is thus not as accurate overall. However, the simulations carried out with our ICCS code provided us with superior statistics by integrating across individual electron spectra as those used in Ref. [12]. The corroboration of the two codes has furthered demonstrated the validity in the described scaling law.

These developments have led to the creation of an alternative to the widely used CAIN code. Using a linear

plane-wave approximation, the resulting scattered spectra can be modeled as a superposition of spectral values for individual electrons [12]. These values are computed by integrating the energy density per angle—given by the product of the time transform of the incident pulse, Compton formula, and cross section—over some defined aperture. In comparison to the Monte Carlo method of evaluating integrals at randomly chosen points, this method proves more accurate. By including improvements in the implementation, the code now runs with the speeds comparable to those of C, yet still benefiting from the clarity and conciseness of PYTHON. The code is still valid only for the low-intensity Compton regime and for a plane-wave approximation of the laser beam. However, the new features of the code provide a foundation for future generalizations to the high-intensity regime and for the paraxial laser pulse approximation [17].

ACKNOWLEDGMENTS

APPENDIX: SECOND-ORDER CORRECTION TO THE SCALING OF THE APERTURE LINEWIDTH GIVEN IN EQ. (14)

For larger apertures, $\gamma\theta_{\max} \approx 1$ and beyond, a uniform distribution may not be an accurate approximation to the spread of scattering angles. The distribution for $\theta_{\max} \ll 1$ is closer to trapezoidal, with vertical bounds $\omega_{\min}$ and $\omega_{\max}$. The slope of the trapezoid matches the slope of distribution at $\theta = 0$, since the range of scattering angles—as dictated by the aperture—remains small. The normalized distribution of frequencies through the aperture $\rho(\omega)$ is thus

$$\rho(\omega) = \frac{2}{(\omega_2 - \omega_1)(\zeta_1 + \zeta_2)}\left(\zeta_1 + \frac{\zeta_2 - \zeta_1}{\omega_2 - \omega_1}(\omega - \omega_1)\right),$$

(A1)

where $\omega_1 = \omega_{\min}$, $\omega_2 = \omega_{\max}$, $\zeta_1 = dN/d\Omega(\theta_{\max})$, and $\zeta_2 = dN/d\Omega(0)$. For this distribution, the following properties are true of the moments of ρ:

$$\langle\omega\rangle = \frac{\zeta_2 - \zeta_1}{\zeta_1 + \zeta_2}\frac{\omega_2 - \omega_1}{6} + \frac{\omega_1 + \omega_2}{2},$$

(A2)

$$\langle\omega^2\rangle = \left(\frac{\omega_1 + \omega_2}{2}\right)^2 + \frac{(\omega_2 - \omega_1)^2}{12}$$
$$+ \frac{\zeta_2 - \zeta_1}{3(\zeta_1 + \zeta_2)}(\omega_2 - \omega_1)\left(\frac{\omega_1 + \omega_2}{2}\right).$$

(A3)

Then the relative rms bandwidth due to the aperture, $\sqrt{\langle\omega^2\rangle - \langle\omega\rangle^2}$, is

$$\frac{\sigma_{\theta_{\max}}}{E_{\theta_{\max}}} = \frac{1}{\sqrt{12}}\frac{\psi^2}{1 + X + \psi^2/2}\sqrt{1 - \frac{1}{3}\left(\frac{\zeta_2 - \zeta_1}{\zeta_1 + \zeta_2}\right)^2}.$$

(A4)

The variance tends to that of a uniform distribution as $(\zeta_2 - \zeta_1)/(\zeta_1 + \zeta_2)$ approaches zero (as the aperture becomes smaller). This second-order correction relies on approximating the values of the electron distribution function $dN/d\Omega(\theta)$ at $\theta = 0$, and $\theta = \theta_{\max}$, which may not be readily available.

---

[1] G. A. Krafft and G. Priebe, Compton sources of electromagnetic radiation, Rev. Accel. Sci. Techol. **03**, 147 (2010).

[2] Z. Huang and R. D. Ruth, Laser-Electron Storage Ring, Phys. Rev. Lett. **80**, 976 (1998).

[3] R. Loewen and R. D. Ruth, in *High-Brightness Sources and Light-Driven Interactions* (Optical Society of America, Washington, DC, 2016), p. ES5A.2.

[4] A. Ovodenko, R. Agustsson, M. Babzien, T. Campese, M. Fedurin, A. Murokh, I. Pogorelsky, M. Polyanskiy, Y. Rozenzweig, J. Sakai, T. Shaftan, and C. Swinson, High duty cycle inverse Compton scattering x-ray source, Appl. Phys. Lett. **109**, 253504 (2016).

[5] A. Bacci *et al.*, Status of the STAR project, Proceedings of the International Particle Accelerator Conference 2016, Busan, Korea, TUPOW004.

[6] O. Adriani *et al.*, Technical design report EuroGammaS proposal for the ELI-NP gamma beam system, arXiv:1407.3669.

[7] C. Vaccarezza *et al.*, The SPARC_LAB Thomson source, Nucl. Instrum. Methods Phys. Res., Sect. A **829**, 237 (2016).

[8] Y. Du, L. Yan, J. Hua, Q. Du, Z. Zhang, R. Li, H. Qian, W. Huang, H. Chen, and C. Tang, Generation of first hard X-ray pulse at Tsinghua Thomson scattering X-ray source, Rev. Sci. Instrum. **84**, 053301 (2013).

[9] H. R. Weller, M. W. Ahmed, H. Gao, W. Tornow, Y. K. Wu, M. Gai, and R. Miskimen, Research opportunities at the upgraded HIGS facility, Prog. Part. Nucl. Phys. **62**, 257 (2009).

[10] R. Hajima and M. Fujiwara, Narrow-band GeV photons generated from an x-ray free-electron laser oscillator, Phys. Rev. Accel. Beams **19**, 020702 (2016).

[11] C. Sun, J. Li, G. Rusev, A. P. Tonchev, and Y. K. Wu, Energy and energy spread measurements of an electron beam by Compton scattering method, Phys. Rev. ST Accel. Beams **12**, 062801 (2009).

[12] G. A. Krafft, E. Johnson, K. Deitrick, B. Terzić, R. Kelmar, T. Hodges, W. Melnitchouk, and J. R. Delayen, Laser pulsing in linear Compton scattering, Phys. Rev. Accel. Beams **19,** 121302 (2016).

[13] J. M. Krämer, A. Jochmann, M. Budde, M. Bussmann, J. P. Couperus, T. E. Cowan, A. Debus, A. Köhler, M. Kuntzsch, A. Laso Garcia, U. Lehnert, P. Michel, R. Pausch, O. Zarini, U. Schramm, and A. Irman, Making spectral shape measurements in inverse Compton scattering a tool for advanced diagnostic applications, Sci. Rep. **8,** 1398 (2018).

[14] I. Ghebregziabher, B. A. Shadwick, and D. Umstadter, Spectral bandwidth reduction of Thomson scattered light by pulse chirping, Phys. Rev. ST Accel. Beams **16,** 030705 (2013).

[15] B. Terzić, K. Deitrick, A. S. Hofler, and G. A. Krafft, Narrow-Band Emission in Thomson Sources Operating in the High-Field Regime, Phys. Rev. Lett. **112,** 074801 (2014).

[16] B. Terzić, C. Reeves, and G. A. Krafft, Combining harmonic generation and laser chirping to achieve high spectral density in Compton sources, Phys. Rev. Accel. Beams **19,** 044403 (2016).

[17] C. Maroli, V. Petrillo, I. Drebot, L. Serafini, B. Terzić, and G. Krafft (to be published).

[18] C. Curatolo, I. Drebot, V. Petrillo, and L. Serafini, Analytical description of photon beam phase spaces in inverse Compton scattering sources, Phys. Rev. Accel. Beams **20,** 080701 (2017).

[19] P. Chen, G. Horton-Smith, T. Ohgaki, A. W. Weidemann, and K. Yokoya, Cain: Conglomérat d'ABEL et d'interactions non-linéaires, Nucl. Instrum. Methods Phys. Res., Sect. A **355,** 107 (1995).

[20] A. H. Compton, A Quantum Theory of the Scattering of X-Rays by Light Elements, Phys. Rev. **21,** 483 (1923).

[21] The Python programming language, http://www.python .org.

[22] S. Behnel, R. Bradshaw, L. Dalcín, M. Florisson, V. Makarov, and D. S. Seljebotn, Cython: C-extensions for Python, http://www.cython.org.

[23] S. Behnel, R. W. Bradshaw, and D. S. Seljebotn, Cython tutorial, in *Proceedings of the 8th Python in Science Conference, Pasadena, CA, 2009*, edited by G. Varoquaux, S. van der Walt, and J. Millman (2009), pp. 4–14, http://conference.scipy.org/proceedings/ scipy2009/SciPy2009_proceedings.pdf.

[24] M. Galassi *et al.*, GNU scientific library reference manual, https://www.gnu.org/software/gsl/.